MODELING OF A LAMINAR DC ARC PLASMA TORCH

Dong-Yan Xu[1], Kai Cheng[1], Xi Chen[1] and Wenxia Pan[2]

[1] Department of Engineering Mechanics, Tsinghua University
Beijing 100084, China. cx-dem@mail.tsinghua.edu.cn
[2] Institute of Mechanics, Chinese Academy of Sciences
Beijing 100080, China. wxpan@imech.ac.cn

ABSTRACT

In recent years, stable and long laminar plasma jets have been successfully generated, and thus it is possible to achieve low-noise working surroundings, better process repeatability and controllability, and reduced metal-oxidation degree in plasma materials processing. With such a recent development in thermal plasma science and technology as the main research background, modeling studies are performed concerning the DC arc plasma torch for generating the long laminar argon plasma jet. Two different two-dimensional modeling approaches are employed to deal with the arc-root attachment at the anode surface. The first approach is based on circumferentially uniform arc-root attachment, while the second uses the so-called fictitious anode method. Modeling results show that the highest temperature and maximum axial-velocity at the plasma torch exit are ~15000 K and ~1100 m/s, respectively, for the case with arc current of 160 A and argon flow rate of 1.95×10^{-4} kg/s.

INTRODUCTION

In thermal plasma materials processing, the thermal plasma jet ejected from a DC arc plasma torch is usually in the turbulent flow state [1,2]. Turbulent plasma jets are always accompanied with large flow fluctuations, intensive noise emission, strong entrainment of surrounding gas into the plasma jets and thus with short lengths of the jet high-temperature region and steep axial gradients of plasma parameters (temperature, axial velocity, etc.) in the jets. These special features of the turbulent plasma jets are often not favourable from the viewpoint of materials processing, because they will worsen the working surroundings of operators, reduce the process repeatability and controllability, and increase the oxidization degree of metallic materials processed in ambient air. In recent years, stable, silent and long laminar plasma jets have been successfully generated using elaborately designed DC arc plasma torches [3-5], and thus a new possibility is provided to achieve low-noise working surroundings, better process repeatability and controllability, and reduced oxidation degree of metallic materials [5,6]. With such a recent development as the main research background, modeling studies are performed concerning the plasma flow and heat transfer within the DC arc plasma torch shown in Fig. 1 used for generating the long laminar plasma jet.

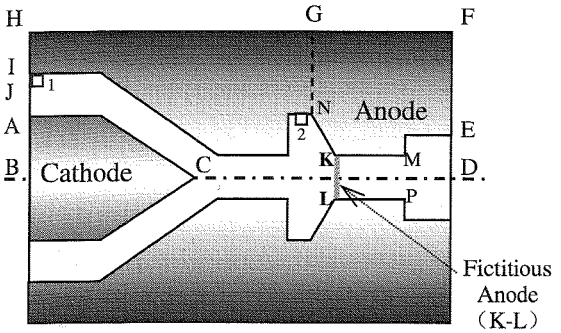

Fig. 1 Schematic of the laminar DC arc plasma torch under study and computational domain

In Fig. 1, the cathode is of 12-mm diameter and 60° cone angle. The solid region on the right hand side of the section G-N is the anode-nozzle with axial length of 26 mm (including a backward step of 8-mm-diameter and 8-mm-length near the exit), while the solid region on the left hand side of the anode is an inter-electrode insert with axial length of 28 mm, which is electrically insulated from the anode and cathode. The central-hole diameter of both the inter-electrode insert and the anode-nozzle is 4 mm. Pure argon is used as the working gas, and the generated plasma jet is issuing into the atmospheric-pressure air surroundings. The working gas is admitted axially and tangentially into the plasma torch around the upstream end of arc cathode (from the inlet section A-I and from tangent hole 1, see Fig. 1) and tangentially from hole 2 near the intersection (G-N) between the inter-electrode insert and the anode.

Close examination of the anode surface after experiments showed that the arc-root attachment at the anode surface is of a diffuse form (circumferentially uniform arc trace is seen at the upstream inclined plane N-K of the anode and near the section K-L), which justifies the employment of a two-dimensional modeling (2D) method in our study. Two different 2D modeling approaches are used to deal with the arc-root attachment at the anode surface in the present study. The first approach is conventional, i.e. based on the assumption that the arc-root attachment at the anode surface is circumferentially uniform [7,8], whereas the second uses the so-called fictitious anode method [9]. When

the first approach is employed, all the cold working gas entering into the plasma torch must pass through the axi-symmetrically distributed arc and be heated directly by the arc. On the other hand, if the arc-root attachment at the anode surface is of a local-attachment form [10], only a part of the cold working gas is directly heated by the arc column itself, while other gas will flow around the arc column and directly towards the exit of anode-nozzle. For such a case, the fictitious anode method [9] may give more reasonable prediction. Predicted results obtained by use of the two different 2D modeling approaches will be compared below.

MODELING APPROACH

The main assumptions employed in this modeling study include that the plasma flow within the plasma torch is steady, laminar and axisymmetrical; the plasma is in the local thermodynamic equilibrium (LTE) state and optically thin to radiation; and the induced electric field is negligible in comparison with the static electric field. The continuity, momentum and energy conservation equations are thus as follows.

$$\frac{\partial}{\partial x}(\rho u)+\frac{1}{r}\frac{\partial}{\partial r}(r\rho v)=0 \quad \text{or} \quad \dot{m} \text{ (at hole 1 and hole 2)} \tag{1}$$

$$\frac{\partial}{\partial x}(\rho uu)+\frac{1}{r}\frac{\partial}{\partial r}(r\rho uv)=-\frac{\partial p}{\partial x}+2\frac{\partial}{\partial x}\left(\mu\frac{\partial u}{\partial x}\right)+\frac{1}{r}\frac{\partial}{\partial r}\left[r\mu\left(\frac{\partial u}{\partial r}+\frac{\partial v}{\partial x}\right)\right]+j_r B_\theta \tag{2}$$

$$\frac{\partial}{\partial x}(\rho uv)+\frac{1}{r}\frac{\partial}{\partial r}(r\rho vv)=-\frac{\partial p}{\partial r}+\frac{\partial}{\partial x}\left[\mu\left(\frac{\partial v}{\partial x}+\frac{\partial u}{\partial r}\right)\right]+\frac{2}{r}\frac{\partial}{\partial r}\left(r\mu\frac{\partial v}{\partial r}\right)-2\mu\frac{v}{r^2}+\rho\frac{w^2}{r}-j_x B_\theta \tag{3}$$

$$\frac{\partial}{\partial x}(\rho ruw)+\frac{1}{r}\frac{\partial}{\partial r}(\rho r^2 vw)=\frac{\partial}{\partial x}\left[\mu\frac{\partial(rw)}{\partial x}\right]+\frac{1}{r}\frac{\partial}{\partial r}\left[r\mu\frac{\partial(rw)}{\partial r}\right]-\frac{2}{r}\frac{\partial(\mu rw)}{\partial r} \tag{4}$$

$$\rho c_p u\frac{\partial T}{\partial x}+\rho c_p v\frac{\partial T}{\partial r}=\frac{\partial}{\partial x}\left(k\frac{\partial T}{\partial x}\right)+\frac{1}{r}\frac{\partial}{\partial r}\left(rk\frac{\partial T}{\partial r}\right)+\frac{j_x^2+j_r^2}{\sigma}-\dot{q}_r+\frac{5}{2}\frac{k_B}{e}\left(j_x\frac{\partial T}{\partial x}+j_r\frac{\partial T}{\partial r}\right) \tag{5}$$

Where u, v and w are the axial (x-), radial (r-) and circumferential (θ-) velocity components; p and T the gas pressure and temperature; ρ, μ, k, c_p, σ and $\dot{q}_r$ are temperature-dependent argon density, viscosity, thermal conductivity, specific heat at constant pressure, electric conductivity and radiation power per unit volume of plasma, respectively. The terms $j_r B_\theta$ and $-j_x B_\theta$ appearing in Eqs. (2) and (3) are the axial and radial components of the Lorentz force, whereas the terms $\frac{j_x^2+j_r^2}{\sigma}$ and $\frac{5}{2}\frac{k_B}{e}\left(j_x\frac{\partial T}{\partial x}+j_r\frac{\partial T}{\partial r}\right)$ on the right hand of Eq. (5) represent the Joule heating rate and the electron enthalpy transport. Here k_B is the Boltzmann constant; e the elementary charge; whereas j_r and j_x are the radial and axial components of the current density, and are related to the electric potential ϕ by $j_r=-\sigma(\partial\phi/\partial r)$ and $j_x=-\sigma(\partial\phi/\partial x)$. The electric potential ϕ is solved using the following current continuity equation

$$\frac{\partial}{\partial x}\left(\sigma\frac{\partial\phi}{\partial x}\right)+\frac{1}{r}\frac{\partial}{\partial r}\left(r\sigma\frac{\partial\phi}{\partial r}\right)=0 \tag{6}$$

while the magnetic induction intensity in the circumferential direction, B_θ, is calculated from

$$B_\theta=\frac{\mu_0}{r}\int_0^r j_x\xi d\xi \tag{7}$$

in which μ_0 is magnetic permeability and $\mu_0 = 4\pi \times 10^{-7}$ H/m.

When the first 2D modeling approach is used, i.e. the arc-root attachment at the anode surface is assumed to be circumferentially uniform [7,8], the boundary conditions employed in the modeling are as follows. At the left end of cathode (A-B), $u = v = rw = 0$, $T =$ 300 K and $\partial\phi/\partial x = I/(A_c\sigma_c)$, where I, A_c and σ_c are the arc current, cathode end area and electric conductivity of cathode material (Sr-W). At the gas inlet section (A-I), $u = Q_1/A_{in}$, $v = 0$, $w = Q_2/(2\pi A_1)$, $T =$ 300 K and $\partial\phi/\partial x = 0$, where Q_1 and Q_2 are the volumetric flow rates of argon admitted axially and tangentially into the torch at A-I and tangent hole 1, A_{in} and A_1 are their inlet areas (the area of hole 1 $A_1 =$ 1 mm^2). Axisymmetrical conditions are employed along the torch axis, i.e. $u = v = rw = 0$, $\partial T/\partial r = 0$ and $\partial\phi/\partial r = 0$ at B-C, while $\partial u/\partial r = 0$, $v = rw = 0$, $\partial T/\partial r = 0$ and $\partial\phi/\partial r = 0$ at C-D. Zero velocities, $T =$ 300 K and zero normal derivative of ϕ are set along the inner surface of the inter-electrode insert, while zero velocities, $T =$ 300 K and $\phi = 0$ are used along the inner surface of the anode-nozzle. One-way boundary conditions (i.e. $\partial u/\partial r = 0$, $\partial v/\partial r = 0$, $\partial(rw)/\partial r = 0$, $\partial T/\partial r = 0$, $\partial\phi/\partial r = 0$) are employed at the torch exit. Working gas also enters into the plasma torch through hole 2, where $w = Q_3/(2\pi A_2)$ is fixed, in which A_2 and Q_3 are the area of hole 2 and the gas volumetric flow rate entering through hole 2. $\dot{m}_1 = \rho Q_2/(2\pi r\Delta r\Delta x)_1$ or $\dot{m}_2 = \rho Q_3/(2\pi r\Delta r\Delta x)_2$ is added into the continuity equation (1) as mass source term at the hole 1 or hole 2 in the computation.

Experimental observation showed that the arc-root attachment at the anode surface is diffuse and located near the section K-L in Fig. 1. Hence, when the second 2D modeling approach (i.e. the so-called fictitious anode method [9]) is employed, the only change in comparison with the first approach described above is that the K-L section is taken as the fictitious anode, and the electric potential in all the plasma region on the right hand of the section K-L is assigned to be zero, besides that at the anode itself.

The variable-property version of the non-commercial program FAST-2D [11] is used to solve Eqs. (1) – (6) with temperature-dependent argon plasma properties. 110 (x-) × 42 (r-) non-orthogonal boundary-conforming grids are employed in the computation.

RESULTS AND DISCUSSION

Typical modeling results are presented in Figs. 2 — 6 for the case with arc current I = 160 A and argon flow rate $Q = Q_1 + Q_2 + Q_3$ = 120 cm^3/s (or 1.95×10^{-4} kg/s, with $Q_1 : Q_2 : Q_3$ = 1 : 1 : 1). Figure 2 and Fig. 3 show the computed temperature and axial-velocity distributions within the plasma torch using the first 2D modeling approach (assuming axisymmetrical arc-root attachment). The highest temperature and the maximum axial-velocity within the plasma torch are ~22000 K and ~ 2000 m/s, respectively. It is seen from Fig. 2 that the high temperature region or the arc zone is located around the axis of the inter-electrode and between the cathode and the upstream end of the anode-nozzle. The predicted location of arc-root attachment at the anode surface (where the arc current is most concentrated) is near the section K-L in Fig. 1, in consistence with the experimental observation mentioned above. On the other hand, the plasma axial-velocity increases rapidly at first, and assumes its maximum within the central part of the plasma torch.

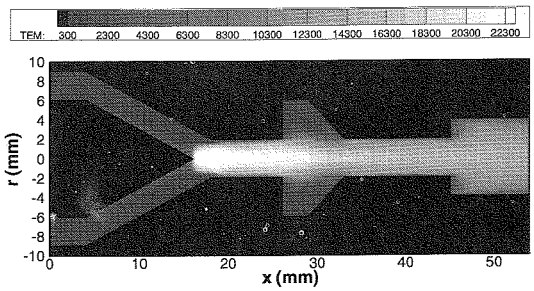

Fig. 2 Computed temperature field within the laminar DC arc plasma torch using the first modeling approach.

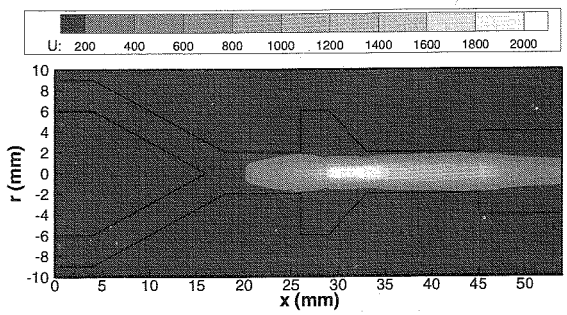

Fig. 3 Computed axial-velocity field within the laminar DC arc plasma torch using the first modeling approach.

Overall similar computed temperature and axial-velocity distributions within the plasma torch are also obtained by use of the second 2D modeling approach, i.e. using the fictitious anode method, although the details of temperature and axial-velocity distributions are somewhat different (not plotted here as separate figures due to the paper space limit).

The predicted plasma temperature and axial-velocity profiles at the downstream end of the 4-mm-diameter nozzle (i.e. at the section MP in Fig. 1) by use of the two different 2D modeling approaches are compared in Figs. 4 and 5. It is expected that these profiles will approximately maintain in the backward step region near the plasma torch, and can be taken as the upstream boundary conditions for the modeling of laminar plasma jet [12]. Figure 4 shows that only small difference exists between the predicted plasma temperature profiles by the two different 2D modeling approaches, with the highest temperature of ~15000 K at the section center. A little difference is also seen in the axial velocity profiles at the section MP shown in Fig. 5, with maximum axial-velocity of 1100 – 1200 m/s at the section center. These predicted results are favorably compared with experimental data. Ref. [6]

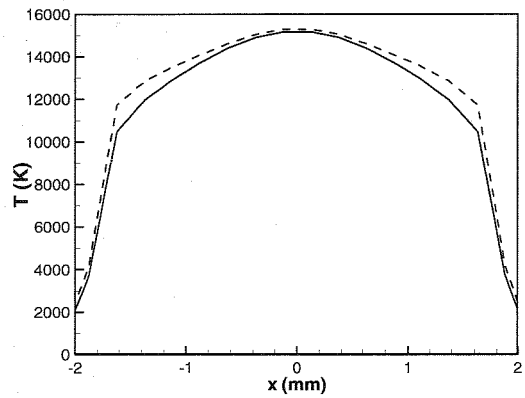

Fig. 4 Comparison of plasma temperature profiles at the section M-P obtained by the two modeling approaches (Continuous line – using the first modeling approach; Broken line – using the fictitious anode method).

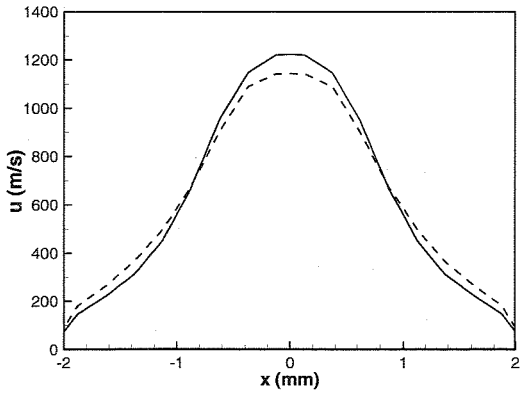

Fig. 5 Comparison of axial-velocity profiles at the section M-P obtained by the two modeling approaches (Continuous line – using the first modeling approach; Broken line – using the fictitious anode method).

showed that for the case with arc current 170 A and mass flow rate 1.95×10^{-4} kg/s, the measured highest temperature near the torch exit section using a spectroscopic method is ~16000 K, whereas the maximum axial-velocity deduced from the measured impact pressure and temperature is ~ 1000 m/s.

The predicted electric potential distributions along the torch axis by the two 2D modeling approaches are compared in Fig. 6. The predicted values of the electric-potential difference between the cathode and anode are ~16.5 V, which is significantly lower than the experimentally measured arc voltage (~ 42 V). The main reason for this discrepancy to appear is that the voltage drops in the cathode sheath and the anode sheath are not included in the present 2D modeling, which will lead to a much lower arc voltage prediction. An acceptable value of the voltage drop in the cathode sheaths is ~ 10 V and that in the anode sheath is a few volts, but the sum of these acceptable voltage drops in the electrode sheaths seems appreciably lower than the observed difference (~25.5 V). However, Ref. [13] reported that an anode voltage drop of 10 ~ 20 V (instead of usually accepted value, i.e. a few volts) was observed for the case with diffuse arc-root attachment at the anode surface. The voltage drops in the cathode and anode sheaths are still open to subsequent studies.

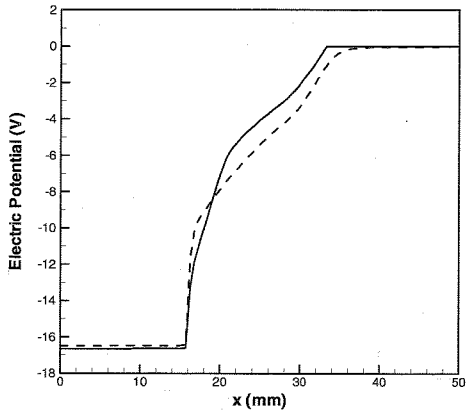

Fig. 6 Comparison of electrical potential distributions along the torch axis (Continuous line – using the first modelling approach; Broken line – using the fictitious anode method).

CONCLUSIONS

Two different 2D modeling approaches give overall similar predicted results concerning the flow and heat transfer within the laminar DC arc plasma torch. For the typical case with arc current 160 A and argon flow rate 120 cm^3/s, the predicted maximum temperature and axial velocity at the downstream end of the 4-mm-diameter anode/nozzle of the plasma torch are approximately 15000 K and 1000 m/s, respectively, which agree reasonably with corresponding experimental data.

ACKNOWLEDGMENT

This work was supported by the National Natural Science Foundation of China (grant Nos. 50336010, 10405015, 10575127).

REFERENCES

[1] E. Pfender, "Thermal plasma technology: Where do we stand and where are we going? ", Plasma Chem. Plasma Process. **19** (1), 1-31 (1999).

[2] P. Fauchais, "Understanding plasma spraying", J. Phys. D: Appl. Phys. **37** (9), R86-R108 (2004).

[3] K. Osaki, O. Fukumasa, "High thermal efficiency-type laminar jet generator for plasma processing", Vacuum **59** (1), 47-54 (2000).

[4] W. X. Pan, W. Hua. Zhang, W. Hong Zhang, C. K. Wu, "Generation of long, laminar plasma jets at atmospheric pressure and effects of flow turbulence", Plasma Chem. Plasma Process. **21** (1), 23-35 (2001).

[5] W. X. Pan, W. H. Zhang, W. Ma, C. K. Wu, "Characteristics of argon laminar DC plasma jet at atmospheric pressure", Plasma Chem. Plasma Process. **22** (2), 271-283 (2002).

[6] W. X. Pan, G. Li, X. Meng, W. Ma, and C. K. Wu, "Laminar plasma jets: Generation, characterization, and applications for materials surface processing", Pure and Applied Chemistry, **77** (2), 373-378 (2005).

[7] D. A. Scott, P. Kovitya, G. N. Haddad, "Temperature in the plume of a dc plasma torch", J. Appl. Phys. **66** (11), 5232-5239 (1989).

[8] R. Westhoff, J. Szekely, "A model of fluid, heat flow, and electromagnetic phenomena in nontransferred arc plasma torch", J. Appl. Phys. **70** (7), 3455-3466 (1991).

[9] J. M. Bauchire, J. J. Gonzalez, A. Gleizes, "Modeling of a DC plasma torch in laminar and turbulent flow", Plasma Chem. Plasma Process. **17** (4), 409-432 (1997).

[10] H.-P. Li, Xi Chen, "Three-dimensional modeling of the flow and heat transfer in a laminar non-transferred arc plasma torch", Chinese Physics, **11** (1), 44-49 (2002).

[11] J. Zhu, FAST-2D: "A computer program for numerical simulation of two-dimensional incompressible flows with complex boundaries", Report No. 690 of the Institute for Hydromechanics, University of Karlsrule (1991).

[12] K. Cheng, Xi Chen, H. –X. Wang, W. X. Pan, "Modeling study of shrouding gas effects on a laminar argon plasma jet impinging upon a flat substrate in air surroundings", Thin Solid Films, **506/507**, 724-728 (2006).

[13] F. M. Curran, D. H. Manzella, "The effect of electrode configuration on arcjet performance", NASA-TM-102346 (1989).